This paper appears in: Dielectrics and Electrical Insulation, IEEE Transactions on, Issue Date: April 2014. Written by: Daily, Connor S.; Sun, Weixing; Kessler, Michael R.; Tan, Xiaoli; Bowler, Nicola. DOI: 10.1109/TDEI.2013.004181

Modeling the interphase of a polymer-based nanodielectric

Abstract

A three-phase theoretical model is proposed that is suitable for describing the effective permittivity of polymer-matrix composites containing spherical nanoparticles. The model accounts for the presence of an interphase region, which surrounds each nanosphere, whose permittivity is allowed to be different from that of the matrix polymer. The nanoparticles themselves are approximated as hard (non-overlapping) spheres, whereas the interphase regions of neighboring nanoparticles are permitted to overlap. The volume fraction of the interphase region is computed by assuming that the nanoparticles are arranged on the nodes of a simple-cubic lattice. The effective permittivity of the composite is subsequently computed via three-phase Wiener bounds. As an example application of the model, permittivity data measured on a silicon/bisphenol E cyanate ester nanodielectric and a low-density polyethylene/alumina nanodielectric are shown to lie outside the range of the two-phase Wiener bounds yet lie within the range of the three-phase Wiener bounds with appropriate choice of interphase permittivity and thickness.

SECTION I.

Introduction

The study of polymer-based dielectrics has been ongoing for the past half century [1], with dielectric relaxations for many main polymer classes being well understood. Chain structure modifications and orientation changes, and their effect on dielectric relaxations, can also be explained. The study of polymer-based nanodielectrics has emerged more recently out of observations of enhanced mechanical and other property improvements in polymer-based nanocomposites. Pioneering work in the field of nanodielectrics was conducted by Nelson et al.[2] in 2002, where epoxy composites filled with nano-sized titania (TiO_2) displayed slightly reduced permittivity values, when compared to their micro-filled counterparts. This lead to the discovery that the titania nanoparticles were inhibiting chain mobility, and the authors began proposing the idea of ‘interaction zones’, a region of highly immobilized chains (1–2 nm) near the filler surface surrounded by highly altered chains that affect composite property changes. In the decade since, the number of works based on the study of polymer-based nanodielectrics has increased significantly, with entire books now devoted to the subject [3].

In 1994, Lewis [4] discussed the phenomenon of an interfacial region that exists between two dielectric media and displays properties that differ from those of its two constituents. As nanofillers of any shape (with at least one dimension less than 100 nm) possess higher surface area-to-volume ratios than their micro-sized counterparts, an interfacial region along the surface of nanofillers is more influential in dictating the properties of the nanocomposite than it is for a microcomposite. In 2004, Lewis again brought interfaces to the forefront of the nanodielectrics

discussion, going so far as deeming interfaces and nanodielectrics 'inextricable' [5]. His proposal of a volumetric, interfacial region was soon termed by many as the 'interphase,' and various attempts were made to characterize its properties and chemistry.

In 2005, Tanaka [6] proposed a multi-core model which divided the interphase into three layers, building upon the two-layered interphase proposed by Tsagaropoulos [7], each with their own unique chemistry, to help describe how the interphase influences nanocomposite properties. In the same year, Roy et al.[8] showed, among other things, that changes in chain mobility, indicative of an interphase presence, can be identified through changes in the glass transition temperature of nanofilled composites. More recently, Raetzke et al.[9] explained improvements in highvoltage arcing resistance of silicone/SiO_2, nanocomposites with an interphase volume model; a model based on nanoparticles with overlapping interphases positioned on the lattice points of a body-centered cubic lattice. Todd and Shi [10] proposed a mixture model based on polarizability calculations to determine the permittivity of an interphase layer, as well as an overlap probability function to determine its thickness. Later, Todd and Shi [11] proposed an interphase power law which calculates the effective composite permittivity using a three-phase power law calculation. Pitsa et al.[12] recently proposed a model to calculate the interphase permittivity, for use in examining how titania nanoparticles affect electrical treeing in epoxy, assuming that the interphase permittivity ranges from particle to matrix permittivity values and varies with respect to an exponential function. Also, Pitsa et al.[13] published a detailed overview of many of the widely accepted theoretical interphase models, including those of Tsagaropoulos and Tanaka.

The proposition of an interphase has been able to help explain certain features or property changes that polymer composites based with nano-sized fillers provide in comparison to their micro-sized counterparts [9]. However, there are still many observations that have yet to be explained. One of these is an anomalous reduction in the relative permittivity of a nanocomposite at low filler loadings, whereby it is reduced below the relative permittivity of the neat, unfilled, matrix material. This anomaly has been shown to present itself in a wide variety of polymer-based nanocomposites, from thermosetting nanocomposites [14]–[15][16][17], to thermoplastic nanocomposites [18], with fillers that may vary in size. The present work attempts to describe 'normal' composite behavior [19], as well as this anomalous behavior, an extension of previous work [20], through the interphase using a multilayered nanofiller model, an approach that has been previously utilized.

Hanai [21] was one of the first to derive basic expressions for the dielectric constant of dispersions of multilayered fillers. In his calculations, Hanai considered a case where spherical particles surrounded by shells of finite thickness were dispersed dilutely in a dispersion medium, with each component of the dispersion having its own volume fraction and complex permittivity. Through this approach, he showed that dispersions of layered, spherical particles experienced two dielectric relaxations, with respect to frequency. A number of previous models have also used a multilayered filler approach to help describe the frequency-based dielectric response of nanocomposites. Steeman *et al.* [22] proposed an interlayer model, based on work derived by Maurer, to help explain dielectric measurements of water adsorption in a glass-bead filled matrix, where the water was represented by the interlayer. Using an approach similar to one which determines various mechanical moduli of polymer-based composites with the interlayer

model, the authors derived an expression which described how the interlayer affected the effective composite permittivity. Similarly, Tinga et al.[23] presented a solution to calculate the complex permittivity of a multiphase mixture, utilizing a confocal ellipsoidal shell that surrounded ellipsoidal nanofillers. Further, first-order effects of neighboring particles were included in the calculations. None of these models account, however, for any overlapping of the interlayer or shell.

We propose a three-dimensional theoretical model, based on a simple-cubic lattice, where monodisperse, inorganic nanoparticles of a finite radius and relative permittivity are fixed on each of the lattice points. Surrounding each nanoparticle in the lattice is an interphase layer of a finite thickness, with its own relative permittivity, which is allowed to overlap with neighboring interphase layers. Volume fractions of the three phases; nanofiller, interphase, and unperturbed matrix material, can be calculated analytically for any nanoparticle loading. Using the results in three-phase Wiener bounds, the effective composite permittivity can be modeled and a range of reasonable values for the interphase thickness and permittivity can be extracted. To the author's knowledge, this is the first work to offer a semi-analytical calculation of the bulk permittivity of a composite with overlapping interphases. The three-dimensional model will first be described in detail in Section 2, followed by an example of the dielectric analysis and extraction of interphase parameters in Section 4. Finally, the interphase parameters (thickness and dielectric constant) are presented for a silicon/bisphenol E cyanate ester nanodielectric, as well as a low-density polyethylene/alumina ($LDPE/Al_2O_3$) nanocomposite system for which the anomalous reduction of permittivity in the nanocomposite, below that of the matrix value, has been observed.

SECTION II.

Model

The three-dimensional theoretical model is proposed based upon hard, spherical nanoparticles with a surrounding interphase layer of discrete thickness that is permitted to overlap with neighboring interphase layers. The nanoparticles are centered on the nodes of a simple cubic lattice, such that three unique phases exist: unperturbed host material, the nanofiller, and the interphase. Calculating the volume fraction of each phase in a composite at a particular nanofiller loading is executed by analyzing a single unit cell of the lattice, side length $2l$. As the nanoparticle radius r_p and interphase thickness t_i are fixed, changes in the nanofiller loading are simulated by changing the size of the unit cell. Due to the geometry of the components of the unit cell, and the unit cell itself, four geometrical regimes arise for different filler loading and interphase thickness pairs, as shown in Figure 1. The calculation of the volume of unperturbed matrix material is provided below for each of the four regimes, and the resulting volume fraction calculations of the three phases follow.

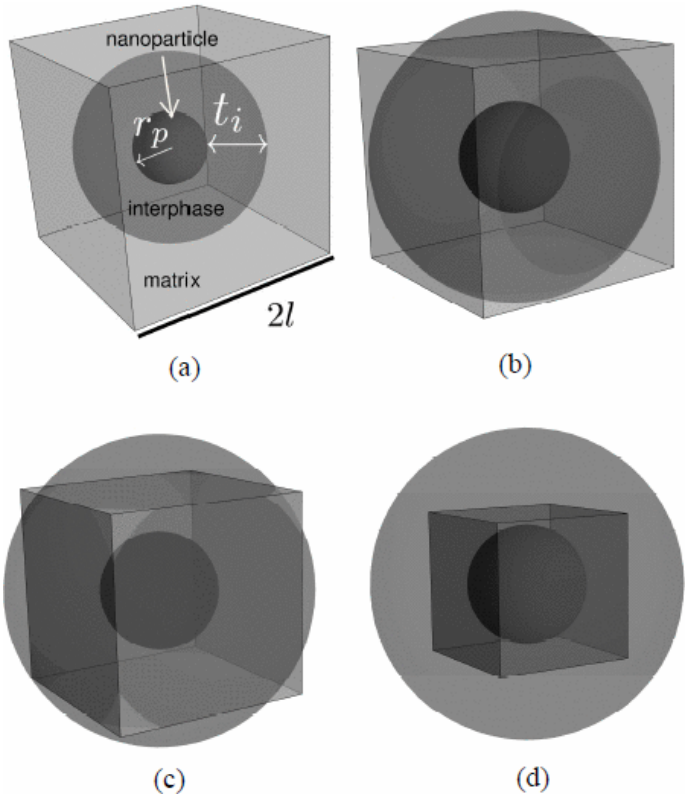

Figure 1. The four geometrical regimes: (a) non-overlapping interphase, (b) interphase overlap through cell faces, (c) interphase overlap through cell faces and edges, (d) matrix displaced entirely by interphase.

A. REGIME ONE: NON-OVERLAPPING INTERPHASE

When the nanofiller loading is low, or when the interphase thickness is extremely small (on the order of a few nanometers), there is likely no interphase overlap. A unit cell representative of Regime One is shown in Figure 1a. To calculate the volume of unperturbed matrix material, the volume of the interphase boundary (nanoparticle + interphase) is simply subtracted from the total unit cell volume. For any pair of nanoparticle radius and interphase thickness, the conditions and the calculation of the unperturbed matrix volume for Regime One are:

$$v_m = 8l^3 - (4/3)\pi r^3; l \geq r$$

where v_m is the unperturbed matrix volume, l is the half length of a side of the unit cell, and r is the radius of the interphase boundary ($r=r_p+t_i$).

B. REGIME TWO: INTERPHASE OVERLAP THROUGH CELL FACES

As the nanofiller loading, or relative size of the interphase thickness, increases beyond those that fall under Regime One, the interphase layers begin to overlap. The overlap is shown in Figure 1b

as six spherical caps protruding from each of the six sides of the unit cell. The volume of unperturbed matrix material can be calculated by using again subtracting the interphase boundary volume from the total unit cell volume, while adding the volume of the six spherical caps, which are no longer inside the unit cell. For any pair of nanoparticle radius and interphase thickness, the conditions and the calculation of the unperturbed matrix volume for Regime Two are:

$$v_m = 8l^3 - \{(4/3)\pi r^3 - 6[(1/3)\pi(r-l)^2(2r+l)]\};$$
$$r/\sqrt{2} \le l \le r$$

C. REGIME THREE: INTERPHASE OVERLAP THROUGH CELL FACES AND EDGES

As the overlap of interphase layers of neighboring nanoparticles begins to increase above that found within the limits of Regime Two, the six spherical caps protruding from each side of the unit cell will begin to overlap with one another along the twelve edges of the unit cell, as shown in Figure 1c. This increased overlap, due to an increase in filler loading or interphase thickness, makes the unperturbed matrix calculation increasingly complex. The material inside the unit cell, a cube with corners that become more, or less, rounded depending on the filler loading and interphase thickness, can be divided into sixteen equal parts. One of these sixteen pieces may be divided into five regions, each with its own volume calculation. The summation of all five regions, for all sixteen pieces, and subsequent subtraction from the total unit cell volume results in the volume of the unperturbed matrix material. The equations for each of the five regions can be found in Appendix A, and the final calculation of the unperturbed matrix material and conditions for Regime 3 are:

$$v_m = 8l^3 - 16(v_{R1} + v_{R2} + v_{R3} + v_{R4} + v_{R5});$$
$$r/\sqrt{3} \le l \le r/\sqrt{2} \le r$$

where v_{R1}–v_{R5} are the volumes of Regions 1–5 described above.

D. REGIME FOUR: MATRIX DISPLACED ENTIRELY BY INTERPHASE

When the nanofiller loading, or interphase thickness to nanoparticle ratio, is relatively high, the interphase extends completely outside the borders of the unit cell, and is indicative of the fourth and final regime, as shown in Figure 1d. Within the unit cell, only two phases now exist: the nanofiller and the interphase. From this simplified case, the calculation for the unperturbed matrix is trivial. This calculation, as well as the nanoparticle and interphase conditions for Regime Four, is

$$v_m = 0; r_p \le l \le r/\sqrt{3} \ge r$$

With the unperturbed matrix volume calculated for all possible scenarios of nanofiller loading, nanofiller radius, and interphase thickness, the volume of the interphase within the unit cell can be calculated by simply taking the total volume of the unit cell, and subtracting the volume of unperturbed matrix material, and the volume of the nanoparticle. Then, the volume fraction of each phase within the unit cell is simply

the volume of each phase contained within the unit cell, divided by the total volume of the unit cell, as shown below,

$$\phi_p = v_p/8l^3; \phi_i = v_i/8l^3; \phi_m = v_m/8l^3$$

where $\phi_p+\phi_i+\phi_m=1$. Plots of the interphase and unperturbed matrix volume fractions with respect to particle volume fraction for a 60 nm radius particle are shown in Figures 2a and 2b, respectively, for select interphase thicknesses.

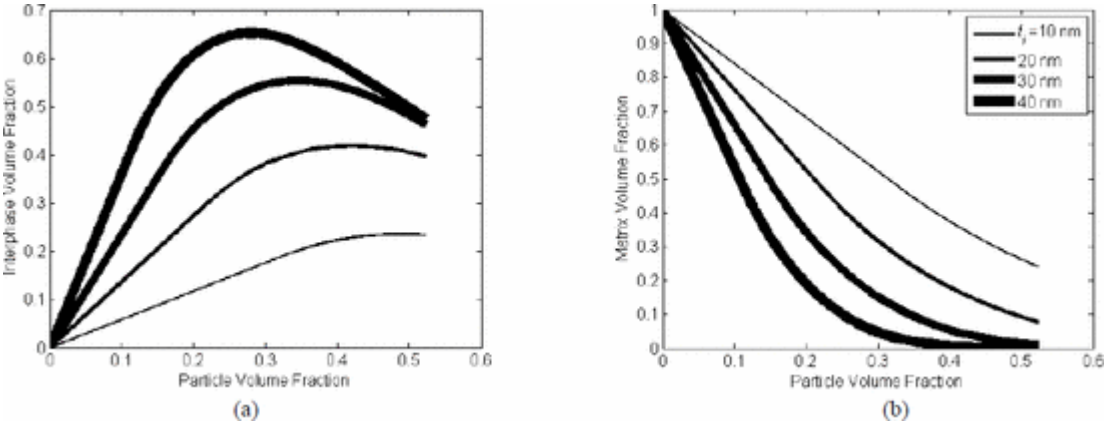

Figure 2. (a) The interphase volume fraction with respect to nanofiller loading and (b) the corresponding unperturbed matrix volume with respect to nanofiller loading for various interphase thicknesses surrounding a 60 nm radius, spherical nanoparticle.

From the shape of the curves in Figures 2a and 2b, a range of nanoparticle loading can be associated with each of the four geometrical regimes. The black curve in both figures can be divided into four different segments. First is a linear segment that is representative of the first regime, and ranges from 0 vol% to low volume fractions. This represents the linear increase of the interphase as particle volume fraction increases. After the linear segment, at slightly higher volume fractions, is a curved segment representative of the second regime that ends at the peak (valley) of the curve. This represents the onset of interphase overlap, and the rate of increase in interphase volume within the unit cell is not as large. The end of this regime corresponds to the limit $l=r/\sqrt{2}$, where the interphase boundary extends exactly to the unit cell edge. The second section of the curved segment is representative of the third regime, where the same section of interphase within the unit cell starts to decrease, due to the increase in particle volume fraction. Finally, the last linear segment (negative slope in Figure 2a) represents the fourth regime, where the unit cell is a two-phase system, comprised of interphase and nanofiller, and the interphase decreases linearly, following the line $y=1-\phi_p$.

E. THREE-PHASE WIENER BOUNDS

The calculated volume fractions for each of the three phases may then be utilized in a three-phase Wiener bound equation to calculate the composite effective permittivity. The Wiener bounds represent the upper and lower limits, respectively, of the effective permittivity of a composite with two or more components, each with their own relative permittivity. Based on the

equivalent capacitance for a set of capacitors connected in parallel and in series, the upper and lower Wiener bounds are, respectively,

$$\epsilon_c = \phi_p \epsilon_p + \phi_i \epsilon_i - \vdash (1 - \phi_p - \phi_i)\epsilon_m$$

$$\frac{1}{\epsilon_c} = \left[\frac{\phi_i}{\epsilon_i} + \frac{\phi_p}{\epsilon_p} + \frac{(1 - \phi_i - \phi_m)}{\epsilon_i} \right]^{-1}$$

where ε_C is the effective composite permittivity, and ε_p;ε_i, and ε_m are the relative permittivities of the nanoparticle, interphase, and unperturbed matrix material, respectively.

SECTION III.

Experiment

Silicon nanoparticles (average particle diameter ~130 nm) were purchased from Nanostructured and Amorphous Materials, Inc., USA. Before composite processing, Si nanoparticles were heat treated in air at 500 °C for 2 hours, resulting in the formation of a continuous surface layer of SiO_2 and to avoid moisture absorption in air. The bisphenol E cyanate ester (BECy) monomer (TenCate Advanced Composites, USA) was mixed with an organometallic-based polymerization catalyst supplied by the manufacturer in a ratio of 100:3. Si nanoparticles were also mixed with BECy monomers to prepare a slurry for composite synthesis. In order to achieve a uniform dispersion of nanofillers, the slurry was ultra-sonicated at 1–2 minute intervals employing a sonic dismembrater (Model 100, Fisher Scientific, USA). Further, the mixture was placed into a planetary mixer (Mazerustar KK50S, KURABO Industries Ltd., Japan) with a simultaneous rotating and de-aerating section for a period of 30 minutes.

The slurry was passed into a 1.1 mm thick steel mold using a 10 mL syringe and was cured in a rotational oven. Disk-shaped samples (diameter 22 mm) containing 10 and 26 vol% of Si nanoparticles were obtained after the curing process and were polished for subsequent dielectric testing.

Fracture surfaces of composite samples were examined by scanning electron microscopy (SEM) (Quanta FEG 250, FEI, USA) to assess the particle dispersion in the polymer matrix. Figure 3 shows the SEM images of the fracture surface of composites with 10 and 26 vol% of Si nanoparticles. It is observed that the nanofillers distribute uniformly in the matrix with little particle agglomeration in the composite with 10 vol% Si loading, shown in Figure 3a. Figure 3b reveals that the dispersion of Si particles at 26 vol% is more variable, with mild agglomeration in some regions. Dielectric properties of the nanocomposites and neat BECy were characterized with a Novocontrol dielectric spectrometer (Novocontrol Technologies, Germany) in a frequency range from 0.01 Hz to 1 MHz at 20 °C.

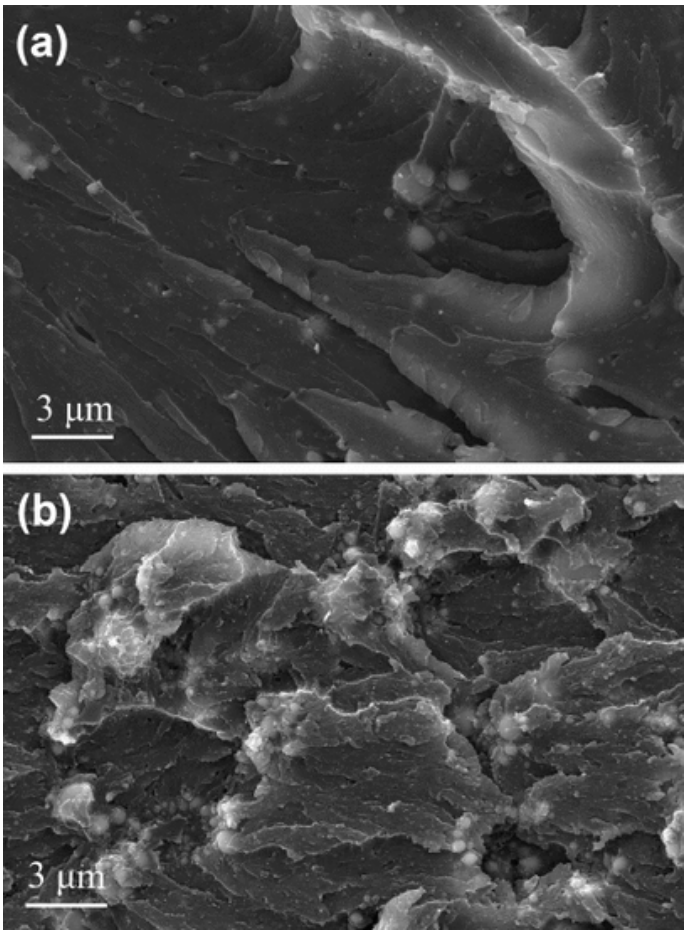

Figure 3. SEM images of the fracture surface of composites with (a) 10 and (b) 26 vol% of Si nanoparticles.

SECTION IV.

Data Analysis

Permittivity data from polymer-based nanocomposites can be analyzed using the volume fraction model and Wiener bounds described in Section 2, along with surface plotting techniques, to extract reasonable values for the interphase thickness and permittivity for a particular nanocomposite system. To proceed, measured relative permittivity values for a nanocomposite at two or more particle volume fractions are needed, as well as the neat matrix and bulk particle permittivity values. With an average particle size, the volume fraction calculations can be performed.

Rather than assigning a particular value to the interphase a range of thicknesses will be used in the calculations, giving a range of volume fraction ratios amongst the three phases. Similarly, rather than assigning a particular value of relative permittivity to the interphase for use in the Wiener bounds, a range of permittivities is utilized. The example surface plot in Figure 4 shows the variation in an effective composite permittivity bound, due to different pairs of interphase

thickness and permittivity, for a particular particle volume fraction. The interphase ranges from 0 nm (no interphase) to 70 nm (extremely large interphase) while the relative interphase permittivity ranges from 1 (air) to ϵ_p.

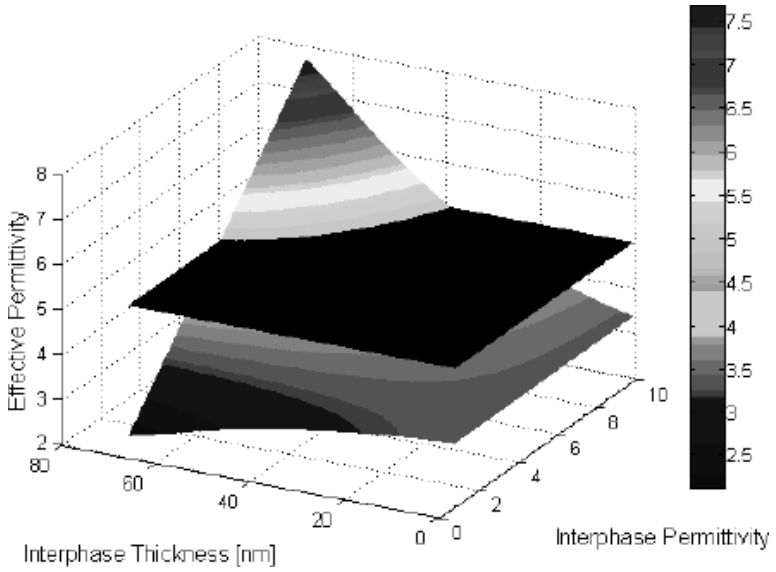

Figure 4. Upper Wiener bound showing the variation in effective permittivity of a nanocomposite as a function of both relative interphase permittivity (ϵi=1−10) and thickness (ti=0−70nm) with intersecting measured permittivity plane (at ϵ=5) at 5 vol% nanofiller. The intersection of the Wiener bound with the plane gives rise to a locus of viable values of ϵi and ti for the interphase. Particle radius=50 nm; particle permittivity =10; matrix permittivity = 3.

Looking at the upper Wiener bound in Figure 4, a few characteristics are worth mentioning. When there is no interphase present (0 nm), the three-phase bound is reduced to a two-phase bound, consisting only of matrix and nanofiller, and the composite permittivity remains constant, as indicated by the horizontal edge along the right-hand axis. Similarly, when the relative interphase permittivity is equal to that of the nanofiller, the upper Wiener bound is again reduced from three-phase to two-phase bounds, and the permittivity increases non-linearly with increased interphase thickness, as shown by the edge along the back of the figure. Finally, if the interphase thickness and/or particle volume fraction is high enough, the fourth Regime will be encountered and the system will turn into a two phase system, this time made of interphase and nanofiller. This is exhibited by the close-to-linear edge in Figure 4, where the interphase thickness is at 70 nm.

With the upper Wiener bound plotted for a particular volume fraction, the measured effective composite permittivity value can now be added to the plot to compare with the bounds. Represented by the black plane, the measured permittivity value is also shown in Figure 4. Any point of intersection between the upper Wiener bound and the measured permittivity plane represents a pair of values for the interphase thickness and permittivity that, when substituted into the volume fraction and three-phase Wiener bound calculations, result in the value of the permittivity measured. The intersections for the same system can be calculated in the same

manner for the lower Wiener bound as well, creating a set of interphase intersection arcs for one volume fraction.

Overlaying two sets of intersection arcs, one for each of two volume fractions, may provide an area of overlap, as indicated by the surface spanned by arrows in Figure 5. Any point within this overlapped area now represents a pair of interphase thickness and permittivity values that satisfy the Wiener bound and volume fraction calculations for both particle volume fractions and corresponding measured permittivity values. Also, this common area of intersection points provides a range of interphase thickness and permittivity values, which represents a more reasonable approach than a single value for each parameter since the ideal assumptions imposed on the volume fraction calculations do not correspond to the non-ideal conditions present in actual composite processing. An example analysis using two sets of measured permittivity values, one experimental [19] and one literature-based [18], is provided below.

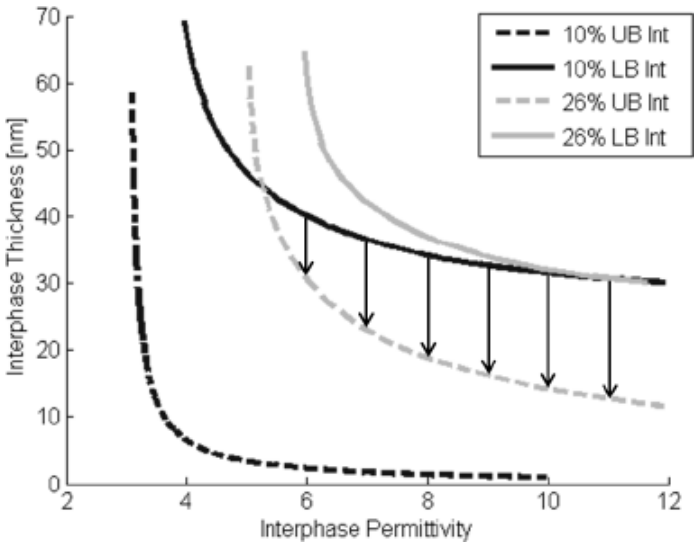

Figure 5. Lines of intersection between calculated three-phase Wiener bounds and measured permittivity values, for two volume fractions of silicon/BECy nanocomposite at 1 MHz. The area highlighted by arrows indicate possible pairs of values for interphase thickness, t_i, and permittivity, ϵ_i, that are common to both volume fractions

A. EXPERIMENT ANALYSIS

Modeled results of the silicion/bisphenol E cyanate ester system described in Section 3 can be seen in Figure 5, where the intersection between the bounds and the permittivity values measured, at two volume fractions, are superimposed upon one another for 1 MHz data. Particle radius 65 nm [19] and relative permittivity 12 [24] were used in the calculations. The matrix relative permittivity was taken as 3.05 at 1 MHz. The area highlighted by arrows indicates pairs of permitted values for interphase thickness, t_i, and permittivity, ϵ_i, that are common to both volume fractions. In Table 1, ranges of acceptable interphase thickness values are listed for various allowable permittivity values, for low (0.01 Hz), medium (113 Hz) and high (1 MHz)

frequency. It can be seen that the allowable interphase permittivity shifts to lower values with increasing frequency, as does that of the BECy matrix [19].

Permittivity data of a low-density polyethylene-alumina (LDPE-Al_2O_3) nanocomposite published by Ciuprina et al.[18] exhibits the anomalous permittivity minimum described earlier. The results from the measurements at 1 kHz were chosen for this analysis, to avoid the effects of charge carriers that might appear in the lower-frequency data. Particle radius 20 nm [18] and relative permittivity 9 [24] were used in the calculations. The matrix relative permittivity was taken as 2.195 at 1 kHz. The results of the analysis can be found in Table 2 below.

Table 1. Example Pairs of Interphase Parameters for which Experimental Data [19] Falls Within Modeled Three-Phase Wiener Bounds.

Frequency	ϵ_i	t_i [nm]
0.01 Hz.	8	34-42
	9	28-40
	10	24-38
	11	21-37
113 Hz.	7	35-41
	8	28-39
	9	22-37
	10	20-37
	11	18-35
1 MHz.	6	32-40
	7	23-37
	8	19-33
	9	17-32
	10	15-31

Table 2. Example Pairs of Interphase Parameters for which Literature Data [18] Falls Within Modeled Three-Phase Wiener Bounds.

ϵ_i	1.2	1.4	1.6	1.8
t_i [nm]	5-13	10-17	12-18	15-22

Based on discussions in [6] on the dimensions of the interphase, all results in which the interphase thickness was calculated to be greater than 30 nm were dismissed from the analysis. All of the results in tables 1 and 2 were not influenced by this dismissal.

In Figures 6 and 7, a single pair of interphase thickness and permittivity values (t_j=30 nm, ϵ_i=7;t_i=15 nm, ϵ_i=1.6, respectively) were chosen from the results of the analysis and substituted

into the volume fraction and three-phase Wiener bound calculations, and subsequently compared to their respective data sets. Similarly, two-phase volume fraction and two-phase Wiener bound calculations were also calculated, using the same values used in the above analysis.

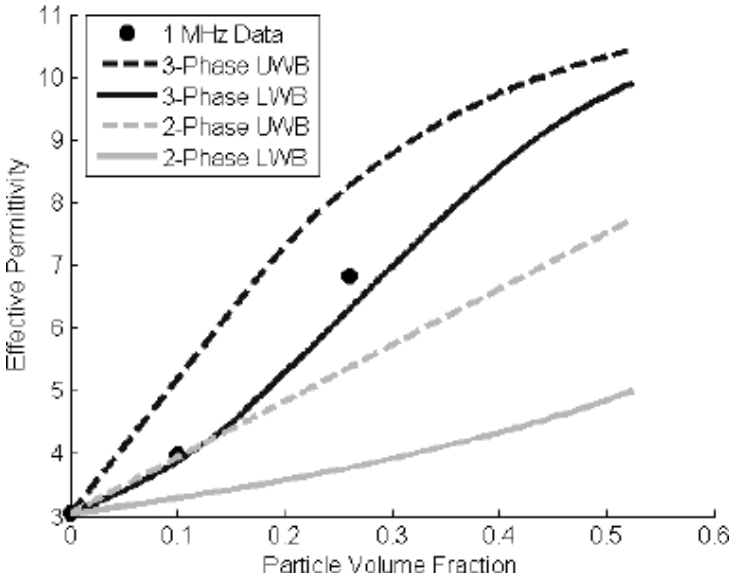

Figure 6. Three-phase and two-phase upper and lower Wiener bounds (UWB and LWB) for 1 MHz permittivity data measured on a silicon/bisphenol E cyanate ester nanocomposite [21]. In the calculation the nanoparticle radius = 65 nm and relative permittivity = 12, while the interphase thickness = 30 nm and relative permittivity = 7.

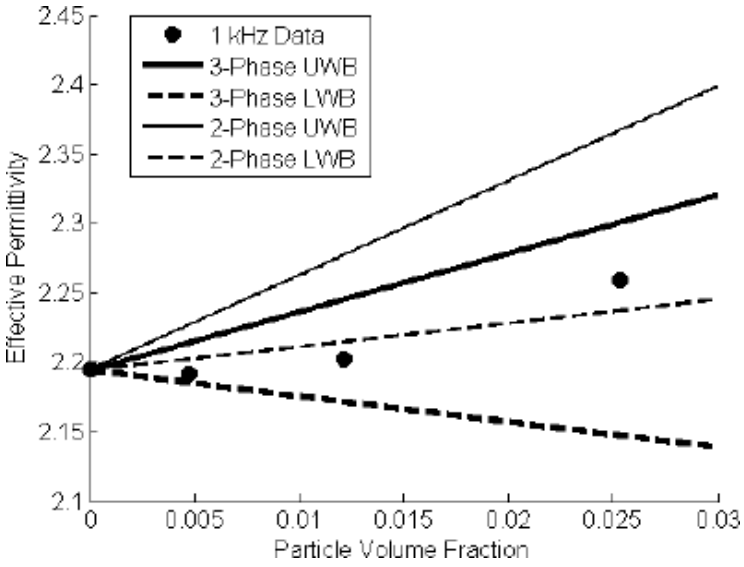

Figure 7. Three-phase (thick curves) and two-phase (thin curves) upper and lower Wiener bounds for 1 kHz permittivity data measured on a LDPE/Al_2O_3 system [16]. In the calculation the nanoparticle radius = 20 nm and relative permittivity = 9, while the interphase thickness = 15 nm and relative permittivity = 1.6.

SECTION V.

Discussion & Conclusions

It can be seen that the data points of two different data sets, one for a thermosetting matrix and one for a thermoplastic matrix, lie within the range of the three-phase Wiener bounds, calculated utilizing reasonable interphase parameters assigned by the procedure described above, while lying outside of the two-phase Wiener bounds. Comparison of the results in Table 1 with results calculated using a previously described model show good agreement. Reference [12] describes interphases with thicknesses around 30 nm (summing all layers for a 25 nm radius particle), which agree with the present results for the BECy/silicon data. Also, Pitsa's model assumes an interphase permittivity ranging between the matrix and nanofiller values, decreasing from the latter exponentially as a function of distance. The present work, while assuming a uniform value for the interphase, also predicts a permittivity value residing between that of the two composite constituents, for the BECy/silicon data, that decreases as the interphase thickness increases.

Comparisons of the results in Table 2 with results using the model found in [12], for LDPE/alumina data that exhibit the anomalous minimum, do not agree, however. While the interphase thicknesses are comparable, depending on the value of interphase permittivity chosen from Table 2, the interphase permittivity values are not. This is due to the anomaly of the minimum permittivity, and the fact that the model in [12] does not account for an interphase permittivity less than that of the matrix, unless a rather large attenuation coefficient is assumed. While the choice of an interphase with permittivity less than that of the matrix results in a better fit to the data, however, a permittivity gradient like that described in [12] is more likely to be realistic.

As previously mentioned, the simple nature of the model allows for a range of interphase parameters to be calculated, an approach that more closely resembles the differences between individual particles within a real composite. However, certain assumptions that insure the simplicity of the model do not simulate realistic conditions. For instance, the constraint that all nanoparticles be fixed on the nodes of a simple-cubic lattice assumes that perfect particle dispersion, free of agglomerations, has taken place, a scenario that often does not occur in real composites. Further, the model constrains the particles, and interphases, to all be uniform in size, respectively, which is also a rare occurrence in practice.

Through the use of randomization techniques, as well as analyzing different microstructures, as opposed to solely spherical particles centered only on a simple-cubic lattice, the authors believe these issues can be dealt with. Starting with the proposed model, the simple-cubic lattice, and respective unit cell, could again be used, except with the constraint that the particle be centered in the unit cell lifted. With the addition of randomly orienting each particle within their respective unit cells, scenarios that more closely resemble actual dispersions can be simulated. However, lifting these constraints also decreases the ease with which the volume fractions can be calculated analytically, assuming the three-dimensional nature is kept intact. Another randomization technique can also be used to more accurately simulate dispersions encountered in practice, by eliminating another constraint from the proposed model: the fixed particle radius. Using a range of particle radii that reflect distributions found in practice would allow for more

realistic permittivity calculations. Again, this makes analytical calculations more complex, though.

Numerical calculations can, however, be utilized in these analytically complex situations. Previous work by Spanoudaki et al.[25] has shown that a randomly generated particle distribution can be utilized in the Maxwell-Garnett mixing model to accurately calculate the permittivity of a composite with spherical inclusions. Also, Brosseau et al.[26] analyzed changes in the effective permittivity due to spherical, rodlike, and ellipsoidal inclusions, as well as their spatial orientation within a unit cell. However, both of these works do not include an interphase layer. The addition of such a layer in both of these numerical analyses could further improve the accuracy of the calculations, as well as provide values for the interphase parameters.

SECTION APPENDIX

CALCULATION OF REGIME 3

As described in Section 2, the calculation of the unperturbed matrix volume fraction is simplified by first dividing the interphase boundary into sixteen identical pieces. Next, each of the sixteenths can be divided into five different regions such that the volume of unperturbed matrix material in the third regime, in which the interphase overlap occurs through cell faces and edges, is expressed in equation (3). The equations for the volume of each of the five regions are listed below, where $c=(l/r)\wedge 2$. The limit θi is also displayed below.

$$v_{R1} = \frac{l^2\sqrt{r^2-2l^2}}{3}$$

$$v_{R2} = \{l^2\sqrt{\frac{r^2-2l^2}{6}}$$

$$v_{R3} = \frac{l^2 r}{3}\left[\frac{(1-c)\tan^{-1}\left[\frac{\sqrt{2c}\sin\theta}{\sqrt{1-2c+\cos(2\theta)}}\right]}{2\sqrt{c}}\right.$$

$$\left.+\frac{\sqrt{1-2c+\cos(2\theta)}\sec\theta\tan\theta}{2\sqrt{2}}\right]_{\theta_i}^{\pi/4}$$

$$v_{R4} = \frac{l^3}{6}\left(\frac{r^2}{l^2}-1\right)\left(\frac{\pi}{4}-\theta_i\right)$$

$$v_{R5} = \frac{r^3}{3}\left[\frac{l}{r}\left(\frac{\pi}{4}-\theta_i\right)-\left(-\sqrt{c}\tan^{-1}\left[\frac{\sqrt{2c}\sin(\theta)}{\sqrt{1-2c+\cos(2\theta)}}\right]\right.\right.$$

$$\left.\left.+\frac{\sqrt{1-c}\sin^{-1}\left[\frac{\sin(\theta)}{\sqrt{1-c}}\right]\sqrt{-\frac{1-2c+\cos(2\theta)}{c-1}}}{\sqrt{1-2c+\cos(2\theta)}}\right)\right]_{\theta_i}^{\pi/4}$$

Where

$$\theta_i = \cos^{-1}\left(\frac{d}{\sqrt{\rho^2 - d^2}}\right)$$

ACKNOWLEDGEMENT

The authors thank Alun Vaughan for his idea for the work, John Bowler for his assistance with volume fraction calculations, and Andrew D. White, Perry E. Antonelli, and Tim E. Cullinan for their help with the analytical solutions. Further information on the formation and calculation of the five regions in Regime Three can be found at http://crowsandcats.blogspot.com/2013/04/cube-sphereintersection-volume.html. This work was funded by NASA Cooperative Agreement No. NNX09AP70A).

References

1. C. Reed, "Advances in polymer dielectrics over the past 50 years", IEEE Electr. Insul. Mag., vol. 29, no.4, pp.58-62, 2013

2. J.K. Nelson, J.C. Fothergill, L.A. Dissado, W. Peasgood, "Towards an understanding of nanometric dielectrics", pp.295-298

3. J.K. Nelson, Springer, 2010

4. T.J. Lewis, "Nanometric dielectrics", IEEE Trans. Dielectr. Electr. Insul., vol. 1, no.5, pp.812-825, 1994

5. T.J. Lewis, "Interfaces are the dominant feature of dielectrics at the nanometric level", IEEE Trans. Dielectr. Electr. Insul., vol. 11, no.5, pp.739-753, 2004

6. T. Tanaka, "Dielectric nanocomposites with insulating properties", IEEE Trans. Dielectr. Electr. Insul., vol. 12, no.5, pp.914-928, 2005

7. G. Tsagaropoulos, A. Eisenberg, "Dynamic mechanical study of the factors affecting the two glass transition behavior of filled polymers. similarities and differences with random ionomers", Macromolecules, vol. 28, no.18, pp.6067-6077, 1995

8. M. Roy, J.K. Nelson, R.K. MacCrone, L.S. Schadler, C.W. Reed, R. Keefe, W. Zenger, "Polymer nanocomposite dielectrics - the role of the interface", IEEE Trans. Dielectr. Electr. Insul., vol. 12, no.4, pp.629-643, 2005

9. S. Raetzke, J. Kindersberger, "Role of interphase on the resistance to high-voltage arcing on tracking and erosion of silicone SiO2 nanocomposites", IEEE Trans. Dielectr. Electr. Insul., vol. 17, no.2, pp.607-614, 2010

10. M. G. Todd, F. G. Shi, "Molecular Basis of the Interphase Dielectric Properties of Microelectronic and Optoelectronic Packaging Materials", IEEE Trans. Compon. Pack., vol. 26, no.3, 2003

11. M. G. Todd, F. G. Shi, "Complex permittivity of composite systems: A comprehensive interphase approach", IEEE Trans. Dielectr. Electr. Insul., vol. 12, no.3, pp.601-611, 2005

12. D. Pitsa, M.G. Danikas, "Modeling relative permittivity and electrical treeing in polymer nanocomposites", Int'l. Sympos. Electr. Insul. Materials, pp.297-300

13. D. Pitsa, M.G. Danikas, "Interfaces features in polymer nanocomposites: A review of proposed models", Nano, vol. 6, no.6, pp.497-508, 2011

14. T. Andritsch, R. Kochetov, Y.T. Gebrekiros, P.H.F. Morshuis, J.J. Smit, "Short term de breakdown strength in epoxy based bn nano-and microcomposites", pp.1-4

15. S. Singha, M.J. Thomas, "Dielectric properties of epoxy nanocomposites", IEEE Trans. Dielectr. Electr. Insul., vol. 15, no.1, pp.12-23, 2008

16. E. Tuncer, I. Sauers, D.R. James, A.R. Ellis, M.P. Paranthaman, T. Aytug, S. Sathyamurthy, K.L. More, J. Li, A. Goyal, "Electrical properties of epoxy resin based nano-composites", Nanotechnology, vol. 18, no.2, pp.1-6, 2007

17. S. Singha, M.J. Thomas, "Reduction of permittivity in epoxy nanocomposites at low nano-filler loadings", pp.726-729

18. F. Ciuprina, I. Plesa, P.V. Notingher, T. Tudorache, "Dielectric properties of nanodielectrics with inorganic fillers", pp.682-685

19. W. Sun, X. Tan, M.R. Kessler, N. Bowler, "Dielectric properties of cyanate ester/silicon nanocomposites for multifunctional structural capacitors", pp.581-584

20. C.S. Daily, M.R. Kessler, X. Tan, N. Bowler, "On the nanoparticle interphase", pp.507-510

21. T. Hanai, P. Sherman, Emulsion Science, Academic Press Inc., 1968

22. P.A.M. Steeman, F.H.J. Maurer, "An interlayer model for the complex dielectric constant of composites", Colloid Polym. Sci., vol. 270, pp.1069-1079, 1992

23. W. R. Tinga, "Generalized approach to multiphase dielectric mixture theory", J. Appl. Phys., vol. 44, pp.3897-3902, 1973

24. D. R. Lide, CRC Press, 2002

25. A. Spanoudaki, R. Pelster, "Effective dielectric properties of composite materials: The dependence on the particle size distribution", Phys. Rev. B, vol. 64, 2001

26. C. Brosseau, A. Beroual, A. Boudida, "How do shape anisotropy and spatial orientation of the constituents affect the permittivity of dielectric heterostructures", J. Appl. Phys., vol. 88, no.12, pp.7278-7288, 2000